A New Spin on Cyclooctatetraene (COT) Redox-Activity: Low-Spin Fe(I) Complexes that Exhibit Antiferromagnetic Coupling to a Singly Reduced η^4-COT Ligand

Tufan K. Mukhopadhyay,[†] Marco Flores,[†] Russell K. Feller,[‡] Brian L. Scott,[‡] R. Dean Taylor,[‡] Moshe Paz-Pasternak,[§] Neil J. Henson,[⊥] Francisca N. Rein,[‖] Nathan C. Smythe,[‖] Ryan J. Trovitch,*[†] John C. Gordon,*[‖]*

[†]*Department of Chemistry & Biochemistry, Arizona State University, Tempe, Arizona 85287*

[‡] *Materials Physics and Applications Division, Los Alamos National Laboratory, Los Alamos, New Mexico 87545*

[§]*School of Physics and Astronomy, Tel Aviv University, 69978 Tel Aviv, Israel*

[⊥]*Theoretical Division, Los Alamos National Laboratory, Los Alamos, New Mexico 87545*

[‖]*Chemistry Division, Los Alamos National Laboratory, Los Alamos, New Mexico 87545*

ryan.trovitch@asu.edu, jgordon@lanl.gov

Abstract Formally zerovalent (κ^3-phosphine)Fe(η^4-COT) complexes supported by either Triphos [$PhP(CH_2CH_2PPh_2)_2$] or Triphos* [$H_3CC(CH_2PPh_2)_3$] have been prepared following chelate addition to $(COT)_2Fe$ (COT = 1,3,5,7-cyclooctatetraene) and by reduction of the respective dibromide complex in the presence of excess COT. The solid state structure of each complex was determined by single crystal X-ray diffraction and close inspection of the metrical parameters revealed significant COT ligand reduction, independent of the coordination geometry about iron. While the neutral and dianionic forms of the redox-active COT ligand have historically received a great deal of attention, a dearth of information regarding the often evoked radical monoanion form of this ligand prompted the full electronic structure investigation of these complexes using a range of techniques. Comparison of the Mössbauer spectroscopic data collected for both (Triphos)Fe(η^4-COT) complexes with data obtained for two appropriate reference compounds indicated that they possess a low-spin Fe(I) center that is antiferromagnetically coupled to a COT radical monoanion. Further evidence for this electronic structure determination by EPR spectroscopy and cyclic voltammetry is presented. Comparing the solid-state metrical parameters determined in this study to related first row transition metal complexes has provides insight into the electronic structure analysis of related organometallic complexes.

Introduction The use of conjugated polyenes as chelates has blossomed over the last half-century, positioning these ligands as primary scaffolds of interest within the field of organometallic chemistry.[1] While polyenes are capable of adopting a range of hapticities upon ligation,[2] one of their more commonly encountered and studied coordination modes remains the *cisoid*-binding of a conjugated diene to a single metal center.[3] Notably, the electronic structure discussion concerning complexes featuring this ligand configuration has focused on the two extremes of diolefin coordination; (a) the neutral diene (L_2) and; (b) the dianionic enediyl (X_2L) modes, the latter of which describes complete two electron reduction of the chelate.[2a] With a

continuum of backbonding into the linear combinations of diene π*-orbitals[2a] possible, transition metal complexes featuring this ligand can adopt an electronic configuration that lies anywhere between the two bonding extremes. This premise has been explored computationally,[4] and seemingly accurate electronic structure descriptions can often be reached following close inspection of crystallographically-determined diene metrical parameters.[3] For example, the solid state structure of (η^4-2-methyl-1,3-butadiene)$_2$Rh(O_3SCF_3) has been found to feature diene ligand olefin distances of 1.406(2), 1.397(2), 1.395(2), and 1.396(2) Å with bridging C-C bond distances of 1.441(2) and 1.443(2)Å,[5] suggesting that each η^4-diene behaves as a neutral ligand as opposed to a dianion. While this approach to electronic structure assignment remains appropriate for many η^4-diene complexes, especially when considering low-spin second and third row complexes that do not exhibit a great degree of backbonding, this methodology remains a drastic oversimplification for complexes of the first transition series, as the possibility for single electron promotion into the lowest energy diene antibonding orbital is often overlooked.

For this reason, an adequate electronic structure investigation of many low-valent first-row metal complexes featuring cyclic η^4-diene ligands has also been impeded. While the electronic descriptions of several complexes supported by η^4-1,3-cyclohexadiene[6] and η^4-naphthalene[7] ligands remain ambiguous, a lack of electronic structure clarity for complexes having a *cisoid*-η^4-COT ligand is especially evident throughout the literature. In a similar manner to acyclic dienes, the coordination chemistry of COT is well established and it had been recognized by the 1960's that this ligand could bind to a transition metal in an η^2,η^2-, η^4-, η^6-, or η^8-fashion.[8] While other binding modes have since been reported,[9] the η^2,η^2- and η^6-coordination modes are well-understood to be neutral in nature (L_2 and L_3, respectively)[2] and the planar η^8-coordination mode is often observed for the dianionic form of this ligand.[10] While poor single crystal X-ray diffraction data has undoubtedly contributed to the inability of researchers to develop clean-cut η^4-COT complex electronic structure divisions (such as those devised for the neutral, radical monoanionic, and dianionic forms of redox-active 2,2'-bipyridine,[11] 2-iminopyridine,[12] and 2,6-bis(imino)pyridine[13] ligands), there happen to be no crystallographically characterized reference compounds that feature an η^4-COT radical monoanion or dianion. Due to the fact that COT tends to be reduced to its dianionic form upon addition of an alkali metal reagent (typically resulting in

μ-η^8,η^8-coordination),[14] isolating and determining the solid-state structure of a compound featuring η^4-COT radical anion coordination to a single alkali metal atom would be an extraordinary achievement. Alternatively, it is conceivable that low-valent, monometallic transition metal complexes exhibiting η^4-coordination to a COT radical anion might be structurally characterized due to their milder redox potentials and capacity to engage in antiferromagnetic coupling.

More than 50 years after Dickens and Lipscomb hinted at the possibility of achieving an η^4-COT electronic structure description that lies somewhere between the neutral diolefin and dianion forms,[15] thoroughly-understood examples of a transition metal complex featuring an η^4-COT radical monoanion ligand have yet to be formulated.[16] In this contribution, two positively identified and structurally characterized complexes of this type are presented and their electronic structures are presented in detail. The potential of this research to provide insight into the electronic structure description of other low-valent η^4-COT supported transition metal complexes is also discussed.

Results While investigating the reduction of (Triphos)FeX_n [Triphos = $PhP(CH_2CH_2PPh_2)_2$; X = Cl, Br; n = 2, 3] with alkali metal reagents, it was found that adding 5 eq. of 2,2'-bipyridine (bpy) to the reaction mixture allowed the preparation of formally zerovalent [κ^3-Triphos]Fe(bpy) (**1-Bpy**), rather than the bis(ligand) product [κ^3-Triphos]Fe[κ^2-Triphos] (**1-κ^2-Triphos**).[17] Since [κ^3-Triphos]Fe(η^4-C_8H_8) (**1-COT**) had previously been prepared by adding an equimolar quantity of Triphos to $Fe(COT)_2$ in benzene-d_6 solution,[18] we hypothesized that this complex could be synthesized upon reducing the corresponding dihalide. Stirring (Triphos)$FeBr_2$ (**1-Br_2**)[17] with excess Na in presence of 10 eq. of COT resulted in the formation of equal quantities of **1-κ^2-Triphos** and **1-COT**. Increasing the amount of added COT to 20 equivalents and conducting the reaction at lower temperatures allowed the isolation of **1-COT** as an analytically pure solid following solvent evaporation and recrystallization (Scheme 1). While it was initially reported that **1-COT** possesses a COT ligand that "is fluxional and presumably η^4-coordinated,"[18] the molecular structure of this complex was sought to verify the COT ligand coordination mode. Layering a concentrated toluene solution of **1-COT** with diethyl ether and allowing the solution to stand at -35 °C afforded single crystals suitable for X-ray diffraction.

The solid state structure determined for **1-COT** (Figure 1), along with the relevant metrical parameters (Table 1), validates the initial assumption that this complex features η^4-COT coordination.

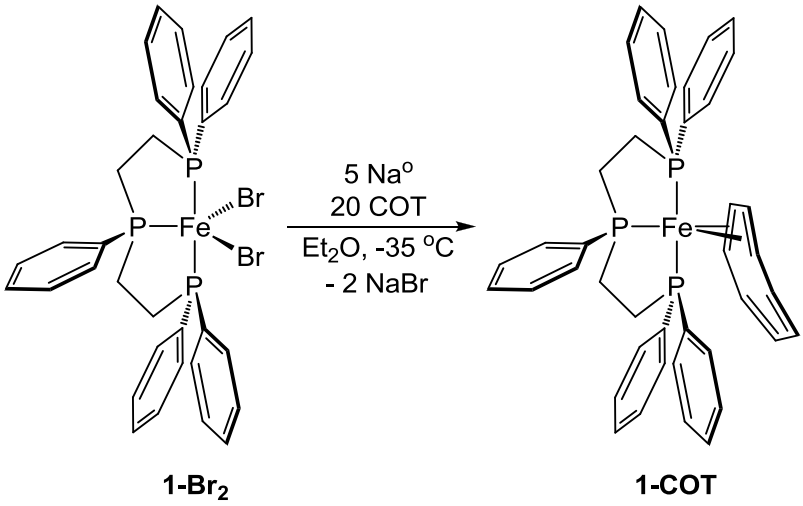

Scheme 1. Synthesis of **1-COT**.

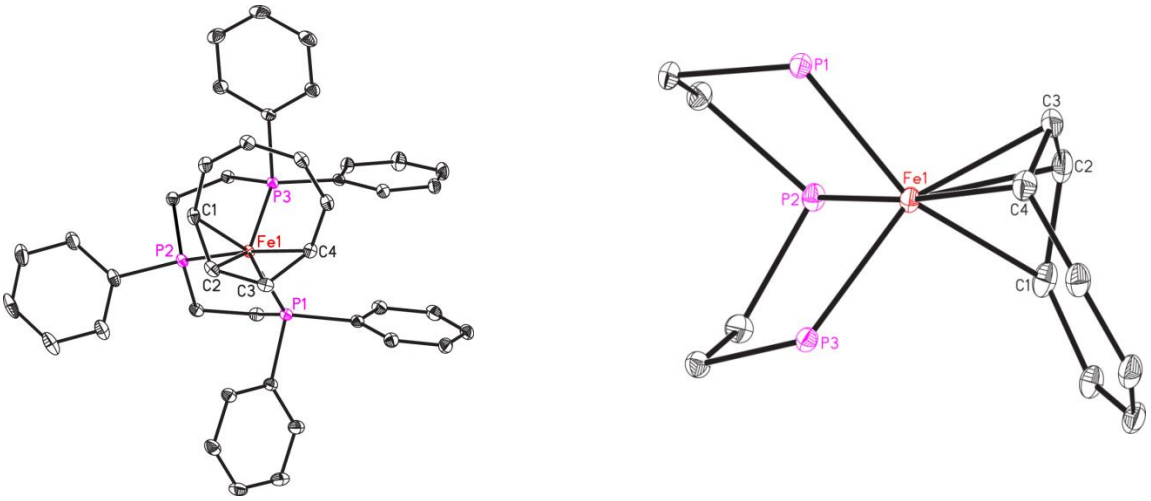

Figure 1. The solid state structure of **1-COT** shown with 30% probability ellipsoids (left). At right, the core of **1-COT** is shown to highlight the overall geometry about iron. Hydrogen atoms and a co-crystallized toluene molecule have been omitted for clarity.

Table 1. Selected bond lengths (Å) and angles (°) for **1-COT** and **2-COT**.

	1-COT	**2-COT**
Fe(1)-P(1)	2.1903(4)	2.1759(8)
Fe(1)-P(2)	2.1758(4)	2.2063(8)
Fe(1)-P(3)	2.1913(4)	2.1909(8)
Fe(1)-C(1)	2.1978(14)	2.233(3)
Fe(1)-C(2)	2.0302(14)	2.047(3)
Fe(1)-C(3)	2.0330(14)	2.059(3)
Fe(1)-C(4)	2.2170(14)	2.265(3)
C(1)-C(2)	1.432(2)	1.426(4)
C(2)-C(3)	1.402(2)	1.391(4)
C(3)-C(4)	1.432(2)	1.429(4)
P(1)-Fe(1)-P(2)	84.929(14)	88.44(3)
P(1)-Fe(1)-P(3)	98.432(15)	91.93(3)
P(2)-Fe(1)-P(3)	86.625(15)	92.99(3)
P(2)-Fe(1)-C(4)	171.60(4)	153.94(8)
P(2)-Fe(1)-C(3)	132.52(4)	97.89(8)
P(2)-Fe(1)-C(2)	99.96(4)	130.47(8)
P(2)-Fe(1)-C(1)	88.79(4)	168.79(7)
C(1)-C(2)-C(3)	125.22(13)	125.4(3)
C(2)-C(3)-C(4)	125.28(14)	125.6(3)

As displayed in Figure 1, the molecular structure of **1-COT** possesses a distorted trigonal bipyramidal geometry about the iron center, with the COT ligand occupying one equatorial [C(1)-C(2)] and one axial coordination site [C(3)-C(4)]. The P-Fe-P angles of 84.929(14), 86.625(15), and 98.432(15) Å deviate from the idealized angles of 90° and 120° while the angle defined by P(2), the iron center and the center of the C(3)-C(4) bond is far from linearity at 152.9°. Importantly, the metrical parameters determined for **1-COT** signify a substantial degree of η^4-COT ligand reduction, as elongation of the C(1)-C(2) and C(3)-C(4) double bonds to 1.432(2) Å each, along with concomitant shortening of the C(2)-C(3) single bond to 1.402(2) Å, is observed. It is also worth noting that the Fe(1)-C(2) and Fe(1)-C(3) bond distances of 2.0302(14) and 2.0330(14) Å found for the internal η^4-COT carbon atoms are much shorter than the Fe(1)-C(1) and Fe(1)-C(4) distances of 2.1978(14) and 2.2170(14) Å, respectively. The uncoordinated COT ligand carbon atoms feature a "localized butadiene" structure with C(5)-C(6), C(6)-C(7), and C(7)-C(8) bond distances of 1.359(2), 1.425(2), and 1.355(2) Å,

respectively, a feature that has been observed for the unbound COT carbon atoms in related iron complexes.[19]

Realizing that the geometry about the metal center in **1-COT** is somewhat atypical, the preparation of a second η^4-COT ligated complex featuring idealized trigonal bipyramidal geometry was targeted to gauge whether geometric considerations play a large role in the degree of crystallographically observed COT ligand reduction, as well as the overall electronic structure determination of such complexes. The Triphos ligand used to support **1-COT** is well-known for its coordinative flexibility and has been found to chelate in either a *fac*- or *mer*-fashion within an octahedral transition metal environment.[20] In order to keep the electronic influence of the chelate consistent, a tied-back variant of this ligand, $H_3CC(CH_2PPh_2)_3$, was chosen due to its rigidity and propensity to coordinate to iron in a *fac*-manner.[21] This ligand is also known as Triphos throughout the literature; however, for the purposes of this manuscript, $H_3CC(CH_2PPh_2)_3$ will be denoted as Triphos* to differentiate it from the more flexible Triphos ligand, $PhP(CH_2CH_2PPh_2)_2$.

Following the methodology first used to prepare and isolate **1-COT**,[18] the stoichiometric addition of Triphos* to $Fe(COT)_2$ in toluene solution allowed the formation of (Triphos*)Fe(η^4-C_8H_8) (**2-COT**), as shown in Scheme 2. Alternatively, this complex could be prepared in a reproducible fashion upon reducing (Triphos*)$FeBr_2$ (**2-Br$_2$**) in the presence 5 eq. of COT (see the Experimental Section). Like **1-COT**, **2-COT** was found to feature one broad ^{1}H NMR resonance for the freely rotating COT ligand at 5.53 ppm and one ^{31}P NMR resonance at 53.35 ppm, indicating that the phosphinoalkyl arms of the Triphos* ligand are equivalent in solution. Additionally, single crystals of **2-COT** suitable for X-ray diffraction were obtained and the solid state structure determined for this complex is displayed in Figure 2.

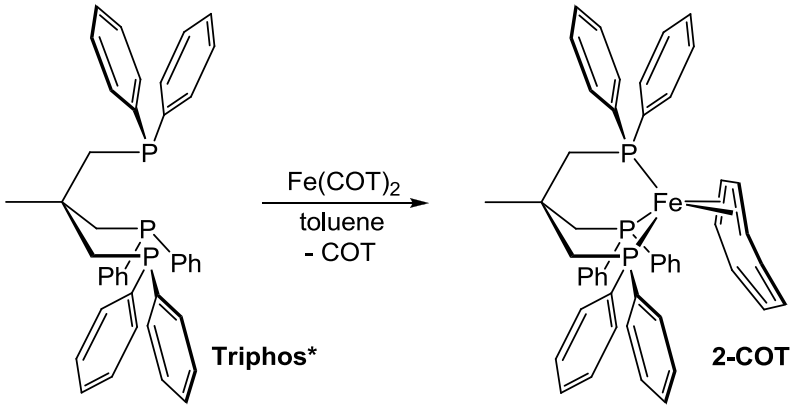

Scheme 2. The synthesis of **2-COT**.

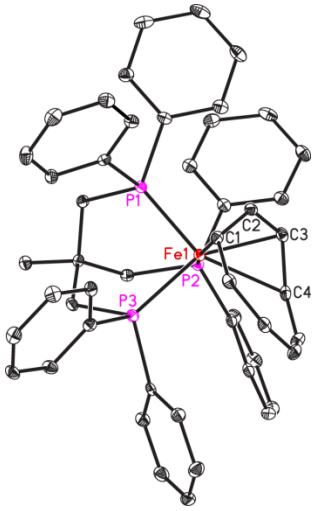

Figure 2.The solid state structure of **2-COT** at 30% probability ellipsoids. Hydrogen atoms have been omitted for clarity.

The metrical parameters determined for **2-COT** (Table 1) reveal P-Fe-P bond angles of 88.44(3), 91.93(3), and 92.99(3)°, indicating that the geometry of the Triphos* chelate as it relates to iron is more representative of an idealized trigonal bipyramid than the angles found for **1-COT**. As with **1-COT**, the COT ligand in **2-COT** occupies one axial and one apical coordination site; however, it should be noted that **2-COT** features an angle defined by P(2), the metal, and the center of the C(1)-C(2) bond that is slightly further from linearity at 150.6°. Although the Fe-P distances determined for **2-COT** of 2.1759(8), 2.1909(8), and 2.2063(8) Å are similar to those found for **1-COT**, the former complex features even longer iron to external η^4-

COT carbon atom bond lengths of 2.233(3) [Fe(1)-C(1)] and 2.265(3) Å [Fe(1)-C(4)]. Importantly, the distances between the bound COT carbon atoms determined for **1-COT** and **2-COT** are statistically indistinguishable, suggesting that a significant amount of electron density is being transferred to the COT ligand from the formally zerovalent iron center in both cases (Table 1).

It has been known for over 50 years that backbonding into (or reduction of) an η^4-COT ligand leads to elongation of the olefin double bonds with concomitant shortening of the bridging C-C single bond as judged by single crystal X-ray diffraction,[15] a feature which has been observed for numerous η^4-COT coordinated complexes (Table 2). At first glance, it is apparent that a wide range of X-ray diffraction data quality is presented in Table 2. With the exception of $[(\eta^4\text{-COT})Cr]_2(\mu\text{-}\eta^5,\eta^5\text{-COT})$[22] and $[(\eta^4\text{-COT})Mo]_2(\mu\text{-}\eta^5,\eta^5\text{-COT})$,[23] most of the crystallographically verified η^4-COT complexes reported over 30 years ago, including $(\eta^4\text{-COT})Fe(CO)_3$,[15] $[(CO)_3Fe]_2(\mu\text{-}\eta^4,\eta^4\text{-COT})$,[15] $(\eta^4\text{-COT})Fe(PPh_3)(CO)_2$,[24] $(\eta^4\text{-COT})Fe(\eta^4\text{-butadiene})(CO)$,[25] $(\eta^4\text{-COT})Zr(\eta^8\text{-COT})(THF)$,[29] $(\eta^4\text{-COT})Ru(CO)_3$,[32] and $[(\eta^4\text{-COT})W]_2(\mu\text{-}\eta^5,\eta^5\text{-COT})$,[31] feature C-C bond distances with estimated standard deviations that are inappropriate for detailed electronic structure discussion.[36] Additionally, the solid state structures determined for $(CO)_3Fe(\mu\text{-}\eta^4,\eta^4\text{-COT})Fe(=COEt(Ph))$,[26] $(\eta^4\text{-COT})_2Fe(BAC)$,[19] $(\eta^4\text{-COT})Zr(\eta^8\text{-COT})$,[28] and $(\eta^5\text{-Cp*})Zr(\mu\text{-}\eta^8,\eta^2\text{-COT})(\eta^4\text{-COT})Zr(\eta^5\text{-Cp*})$[30] possess a significant degree of C-C distance uncertainty within the COT ligand. The metrical parameters determined for $[(\eta^8\text{-COT})Ti]_2(\mu\text{-}\eta^4,\eta^4\text{-COT})$[37] and $[(2,6\text{-}(2,6\text{-}^i Pr_2\text{-}C_6H_3)C_6H_3)Cr]_2(\mu\text{-}\eta^3,\eta^4\text{-COT})$[38] have been excluded from Table 2 since these complexes feature unusual $\mu\text{-}\eta^4,\eta^4$-COT and $\mu\text{-}\eta^3,\eta^4$-COT binding modes, respectively, in which one or more of the η^4-COT carbon atoms are coordinated to both metal centers. While population of the lowest lying COT π^*-orbital might not be achieved for the second and third row complexes shown in Table 2, it is important to note that several of the first row complexes listed feature significant C(1)-C(2)/C(3)-C(4) bond elongation with concomitant C(2)-C(3) bond shortening, indicating that they could in fact have an electronic structure best described as having an η^4-COT radical monoanionic or dianionic ligand.

Table 2. Selected bond lengths (Å) for complexes featuring η^4-COT coordination. Distances shown in italics are excluded from electronic structure discussion throughout the text.[36]

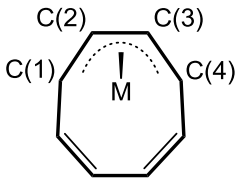

Complex	**C(1)-C(2)**	**C(2)-C(3)**	**C(3)-C(4)**	**Ref.**
$[(\eta^4\text{-COT})Cr]_2(\mu\text{-}\eta^5,\eta^5\text{-COT})$	1.388(6)	1.398(5)	1.375(7)	22
	1.387(5)	1.407(5)	1.427(5)	
$(\eta^4\text{-COT})Fe(CO)_3$	*1.42(1)*	*1.42(2)*	*1.42(1)*	15
$[(\eta^4\text{-COT})Fe(CO_3)]_2[((\mu\text{-}\eta^1,\eta^1\text{-}(N,N)\text{-}$	1.446(8)	1.378(9)	1.421(8)	23
$2,4\text{-}(CF_3)_2N_2C_3)Ag]_3$	1.443(9)	1.393(9)	1.399(9)	
$[(CO)_3Fe]_2(\mu\text{-}\eta^4,\eta^4\text{-COT})$	*1.43(3)*	*1.39(4)*	*1.40(4)*	15
	1.48(4)	*1.40(4)*	*1.44(3)*	
$(\eta^4\text{-COT})Fe(PPh_3)(CO)_2$	*1.449(9)*	*1.417(10)*	*1.450(8)*	24
$(\eta^4\text{-COT})Fe(\eta^4\text{-butadiene})(CO)$	*1.412(7)*	*1.388(16)*	*1.412(7)*	25
$(CO)_3Fe(\mu\text{-}\eta^4,\eta^4\text{-COT})Fe(=COEt(Ph))$	*1.47(3)*	*1.36(3)*	*1.40(3)*	26
	1.48(3)	*1.41(3)*	*1.43(3)*	
$(\eta^4\text{-COT})Fe(BAC)_2$[a]	1.415(5)	1.382(6)	1.429(6)	19
$(\eta^4\text{-COT})_2Fe(BAC)$[a]	*1.387(13)*	*1.421(12)*	*1.419(13)*	19
	1.375(14)	*1.430(14)*	*1.376(14)*	
$(\eta^4\text{-COT})Fe(\eta^4,\eta^2\text{-cyclooctatriene})_2$[b]	1.4201(16)	1.4049(16)	1.4224(15)	19
$(\eta^4\text{-COT})Fe(\mu\text{-}\eta^5,\eta^5\text{-COT})Fe(R)$[c]	1.447(3)	1.400(3)	1.400(4)	19
(Triphos)Fe(η^4-COT) (**1-COT**)	1.432(2)	1.402(2)	1.432(2)	This Work
(Triphos*)Fe(η^4-COT) (**2-COT**)	1.426(4)	1.391(4)	1.429(4)	This Work
$[(\eta^4\text{-COT})_2Co][K(2,2,2\text{-crypt})]$	1.429(4)	1.398(4)	1.437(4)	27
$(\eta^4\text{-COT})Zr(\eta^8\text{-COT})$	*1.40(2)*	*1.39(2)*	*1.40(2)*	28
$(\eta^4\text{-COT})Zr(\eta^8\text{-COT})(THF)$	*1.36(3)*	*1.44(3)*	*1.45(2)*	29
$(\eta^5\text{-Cp*})Zr(\mu\text{-}\eta^8,\eta^2\text{-COT})(\eta^4\text{-}$	*1.42(1)*	*1.37(1)*	*1.41(1)*	30
$COT)Zr(\eta^5\text{-Cp*})$				
$[(\eta^4\text{-COT})Mo]_2(\mu\text{-}\eta^5,\eta^5\text{-COT})$	1.425(8)	1.416(8)	1.416(9)	31
	1.432(9)	1.398(10)	1.427(10)	
$(\eta^4\text{-COT})Ru(CO)_3$	*1.443(8)*	*1.394(12)*	*1.443(8)*	32
$[(\eta^5\text{-Cp})Ru(\mu\text{-}\eta^4,\eta^4\text{-COT})(\mu\text{-H})Ru(\eta^5\text{-}$	1.418(2)	1.428(4)	1.418(2)	33
$Cp)][PF_6]$				
$[(\eta^5\text{-Cp})Ru]_2(\mu\text{-}\eta^4,\eta^4\text{-COT})$	1.455(4)	1.428(5)	1.430(5)	33
	1.424(5)	1.425(5)	1.426(5)	
$[(CO)_2Ru]_2(\mu\text{-}\eta^4,\eta^4\text{-COT})(\mu\text{-}\eta^1,\eta^1\text{-CO})$	1.401(6)	1.412(7)	1.409(8)	34
$[(\eta^5\text{-Cp})Rh(\mu\text{-}\eta^4,\eta^4\text{-COT})Rh(\eta^2,\eta^2\text{-}$	1.423(5)	1.405(8)	1.423(5)	35
$norbornadiene)][BF_4]$	1.425(5)	1.420(8)	1.425(5)	
$[(\eta^4\text{-COT})W]_2(\mu\text{-}\eta^5,\eta^5\text{-COT})$	*1.38(3)*	*1.46(3)*	*1.41(3)*	29
	1.43(4)	*1.37(4)*	*1.47(4)*	

[a]BAC = *N*,*N*-bis(diisopropyl)aminocyclopropenylidene. [b]The 5- and 8-positions of the cyclooctatriene ring are bridged by a quaternary carbon atom that lies in the 2-position of an *N*-(2,6-diisopropylphenyl)-3,3,5,5-tetramethylpyrrolidine ring. [c]R = 2,4-(*N*,*N*)-bis(2,6-diisopropylphenyl-3,5-diphenylimidazole.

Since the crystallographically determined metrical parameters for **1-COT** and **2-COT** suggest that these complexes might have a singly or doubly reduced COT ligand with a non-zerovalent metal center, further spectroscopic study was sought before arriving at a final electronic structure description. Because the electronic structures of **1-κ^2-Triphos** and **1-Bpy** are well-understood (Scheme 3),[17] these complexes were chosen as reference compounds for the Mössbauer spectroscopic investigation of **1-COT** and **2-COT**. The Mössbauer spectrum of **1-κ^2-Triphos** (See Figure S1 of the Supporting Information) was recorded at 77 K and was found to feature an equal abundance of geometrically distinct components characterized by isomer shift values (IS or δ) of 0.07 and 0.09 mm/s and quadrupole splitting parameters (ΔE_Q) of 2.00 and 2.13 mm/s, respectively (Table 3). The Mössbauer spectrum of **1-κ^2-Triphos** was also found to feature a small amount of an iron containing impurity that grows in upon prolonged exposure to air. The values obtained for **1-κ^2-Triphos** are comparable to those obtained for $Fe(CO)_5$ (δ = -0.09 mm/s, ΔE_Q = 2.57 mm/s),[39] such that the differences in isomer shift and quadrupole splitting between the complexes reflect the relative ligand field strength about iron.[40] Like $Fe(CO)_5$,[41] **1-κ^2-Triphos** was found to possess a near trigonal bipyramidal geometry in the solid state (see Figure S5 and Table S4 of the Supporting Information).

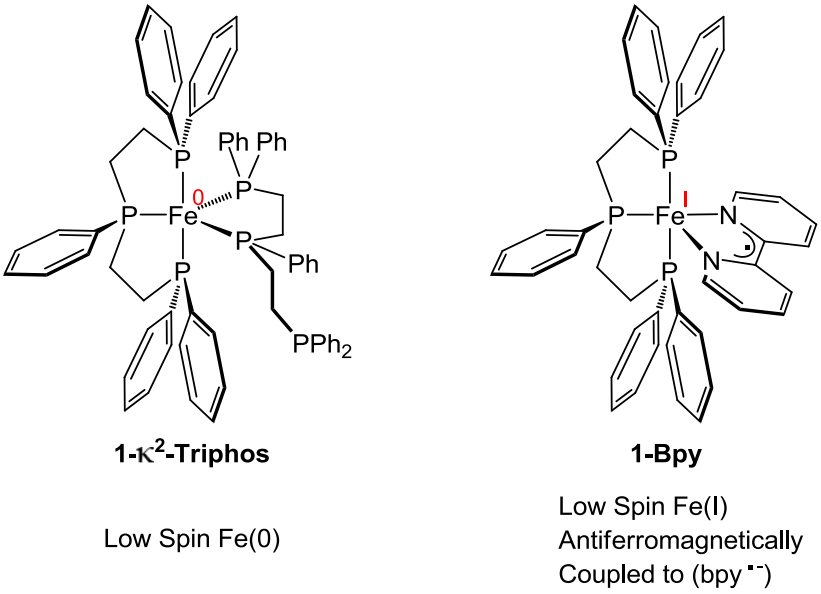

Scheme 3. The electronic structure representation of **1-κ^2-Triphos** and **1-Bpy**.

Table 3. Mössbauer parameters for complexes discussed in this study.

	IS (1) (mm/s)	ΔE_Q (1) (mm/s)	IS (2) (mm/s)	ΔE_Q (2) (mm/s)	Fe(1)/Fe(2) Relative Abundance (%)
1-κ^2-Triphos	0.09	2.00	0.07	2.31	50.5/49.5
1-Bpy	0.06	1.35	0.04	1.04	65.6/34.4
1-COT	0.11	1.08	-	-	100
2-COT	0.16	1.05	-	-	100

The Mössbauer spectrum of **1-Bpy** (Figure S2 of the Supporting Information), which is known to have an electronic structure consistent with a monoreduced bpy chelate that antiferromagnetically couples to an Fe(I) center,[17] features two geometrically distinct components with isomer shifts that are similar to the ones determined for **1-κ^2-Triphos**. Although the isomer shift parameter of high spin iron complexes often allows for an accurate oxidation state determination, this observation was not surprising since minimal isomer shift differences are known to exist between low-spin iron complexes with varying oxidation states.[40] On the other hand, the quadrupole splitting parameters determined for **1-Bpy** (1.04 and 1.35 mm/s) are significantly smaller than the values found for **1-κ^2-Triphos** (2.00 and 2.31 mm/s),

suggesting that the former complex has a diminished electric field gradient due to the removal of one iron-based electron.

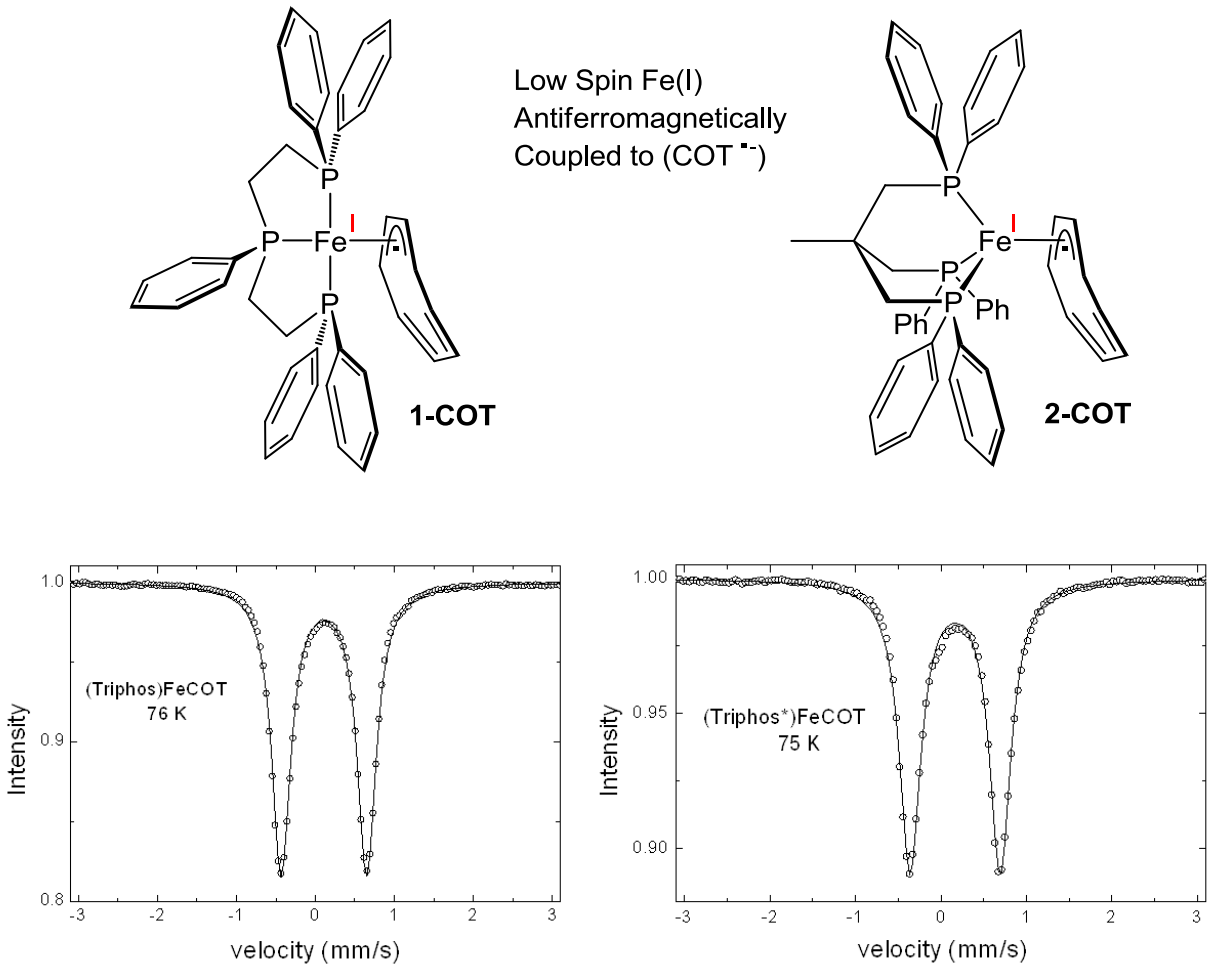

Scheme 4. The electronic structure representations (top) and Mössbauer spectra (bottom) of **1-COT** and **2-COT**.

As with the reference compounds, the Mössbauer spectrum of **1-COT** (Scheme 4, left) was found to feature an undistinguished isomer shift of 0.11 mm/s due to its low-spin configuration.[39] However, the quadrupole splitting parameter of 1.08 mm/s determined for this complex is even smaller than the values found for **1-Bpy** (Table 3), consistent with a reduction in the iron d-electron count. Although a slightly higher isomer shift of 0.16 mm/s was found for **2-COT**, this complex also exhibited a diminished quadrupole splitting of 1.05 mm/s. For this reason, it is believed that the electronic structures of **1-COT** and **2-COT** are consistent with an η^4-COT

radical monoanion that is antiferromagnetically coupled to a low-spin Fe(I) center, as displayed at the top of Scheme 4.

To obtain additional supporting evidence for the electronic structure determination of **1-COT**, the X-band (9.45 GHz) electron paramagnetic resonance (EPR) spectra of this complex was recorded in a toluene glass over a range of cryogenic temperatures. The EPR spectrum of **1-COT** was found to contain a signal with seven-line splitting between 4 K and 130 K (Figure 3b). Expectedly, this signal pattern deviates significantly from what would be expected for a single spin center (S = ½) and the positions and relative amplitudes of the peaks are not consistent with those measured for a typical triplet state (S = 1). The EPR pattern observed for **1-COT** is similar to those previously reported for systems with two S = 1/2 spins coupled by weak exchange and dipole-dipole interactions.[42] Within this model, both the triplet and singlet states are active (Figure 3a). To ascertain whether the EPR spectrum of **1-COT** corresponds to such a spin system, the respective spin Hamiltonian was fit to the data (Figure 3b, dashed line) while assuming that one spin belongs to the unpaired electron of a low-spin Fe(I) center and the second belongs to an unpaired electron located within the η^4-COT ligand (Fe^{1+}-$COT^{\bullet -}$), as displayed in Figure 3.

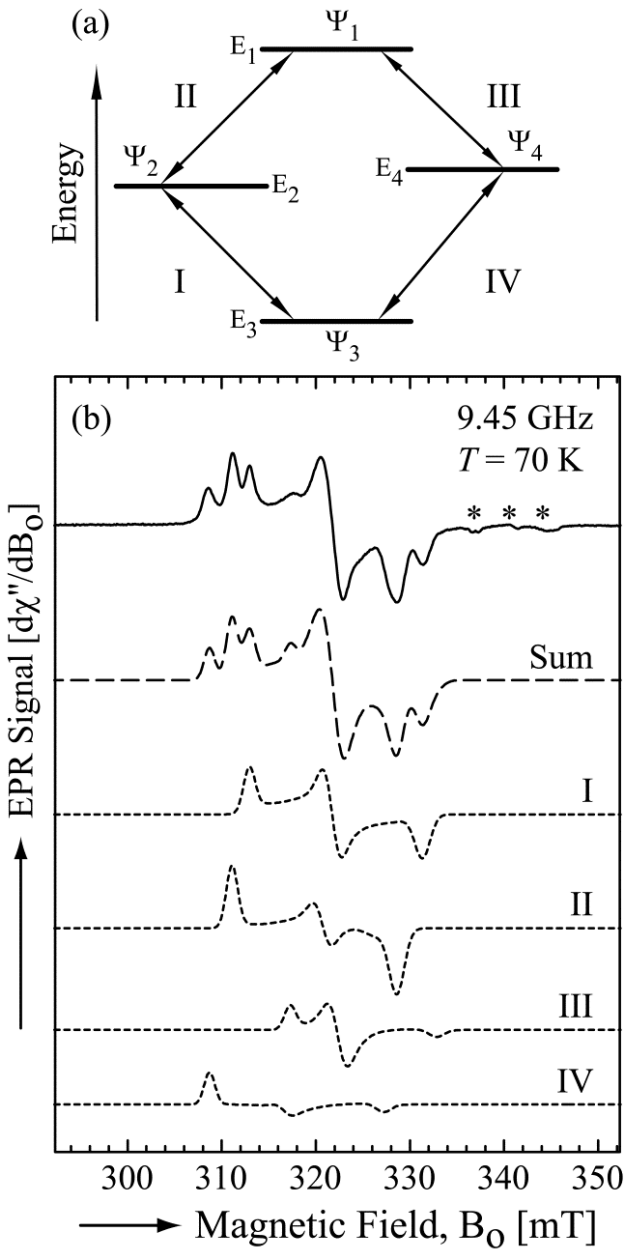

Figure 3. (a) Energy levels (E_i) of the eigenstates (Ψ_i) for the coupled metal-radical spin-dimer (Fe^{1+}-$COT^{\bullet -}$). The eigenstates of the triplet state are: $\Psi_1 = |+ +\rangle$, $\Psi_2 = a|+ -\rangle + b\,|- +\rangle$ and $\Psi_3 = |- -\rangle$, the one of the singlet state is: $\Psi_4 = -b|+ -\rangle + a\,|- +\rangle$. The allowed transitions between these levels (I, II, III, and IV) are indicated by arrows. (b) Experimental (solid line) and simulated (dashed line) EPR spectra of **1-COT**. The small lines at higher field (marked with *) belong to minor impurities. Simulation of the spectral components corresponding to transitions I, II, III, and IV of randomly oriented Fe^{1+}-$COT^{\bullet -}$ spin-dimers (i.e., as obtained in frozen solutions) are also shown (dotted lines). The sum of the spectral components (dotted lines) results in the simulated spectrum (dashed line).

The spectral features observed for **1-COT** were well-fit (σ = 2.3%, see Experimental Section for the definition of σ) when treating this complex as an Fe^{1+}-$COT^{\bullet -}$ spin-dimer and the parameters that were obtained are summarized in Table 4. The magnitude of the isotropic exchange interaction J_o (-70.7 MHz) is small. This is consistent with the model used to fit the data and shows no significant overlapping between the wave functions corresponding to the unpaired electrons (two) within **1-COT**. Furthermore, the principal components of the dipole-dipole interaction tensor ($J_{x'}$ = 141.8 MHz, $J_{y'}$ = -101.1 MHz, $J_{z'}$ = -40.7 MHz) are relatively large and significantly deviated from axial symmetry. These properties reflect a strong dipolar interaction between the two unpaired electrons which is due to their close proximity. Thus, the EPR results at cryogenic temperatures provide strong evidence that the electronic structure of **1-COT** is best described as having an Fe(I) center that is coordinated to a COT radical monoanion.

Table 4. Parameters used in fitting of the EPR spectrum of **1-COT** (Fe^{1+}-$COT^{\bullet -}$) in a toluene glass at 9.45 GHz and T = 70 K.

Parameter[a]	Fe^{1+}-$COT^{\bullet -}$
J_o (MHz)	-70.7
$J_{x'}$ (MHz)	141.8
$J_{y'}$ (MHz)	-101.1
$J_{z'}$ (MHz)	-40.7
$\frac{1}{2}(g_{xA} + g_{xB})$	2.153
$\frac{1}{2}\lvert g_{xA} - g_{xB}\rvert$[b]	0.016
$\frac{1}{2}(g_{yA} + g_{yB})$	2.115
$\frac{1}{2}\lvert g_{yA} - g_{yB}\rvert$[b]	0.000
$\frac{1}{2}(g_{zA} + g_{zB})$	2.046
$\frac{1}{2}\lvert g_{zA} - g_{zB}\rvert$[b]	0.009
ΔB_x (MHz)	39.0
ΔB_y (MHz)	58.1
ΔB_z (MHz)	54.1

[a]See the Experimental Section for the definition of the fitting parameters. [b]Specific g-values to either Fe^{1+} or $COT^{\bullet -}$ cannot be assigned due to the multiple solutions obtained for these parameters. For this reason Table 4 contains only the absolute values of the differences $|g_{iA} - g_{iB}|$.

Cyclic voltammetry experiments were also conducted on **1-COT** and **2-COT**. The voltammogram of **2-COT** in THF showed three reversible redox processes (Fig. 4), and differential pulse voltammetry confirmed that each of these processes involves the same number

of electrons. Starting from the complex in its isolated redox state (Fe^{I},COT^{-}), the first reduction with $E_{1/2}$ at -2.74 V (vs Fc/Fc^{+}) is assigned to the metal-based Fe^{I}/Fe^{0} couple, while the first oxidation at -2.09 V corresponds to the ligand-based COT^{-}/COT^{0} couple. The second oxidation with mid-potential at -0.25 V is assigned to the metal-based Fe^{I}/Fe^{II} couple. Although the reverse process (Fe^{II}/Fe^{I}) is observed on the timescale of voltammetry, sustained application of a potential > -0.2 V showed that the oxidized Fe^{II},COT^{0} species is chemically unstable. The analogous three processes were also observed for **1-COT**, but the overall electrochemical behavior proved to be more complicated in this case. As shown in Fig. S6, only the first oxidation (COT^{-}/COT^{0} couple) is fully reversible with $E_{1/2}$ = -2.24 V, while both the first reduction (Fe^{I}/Fe^{0}) and second oxidation (Fe^{I}/Fe^{II}) processes are electrochemically irreversible.

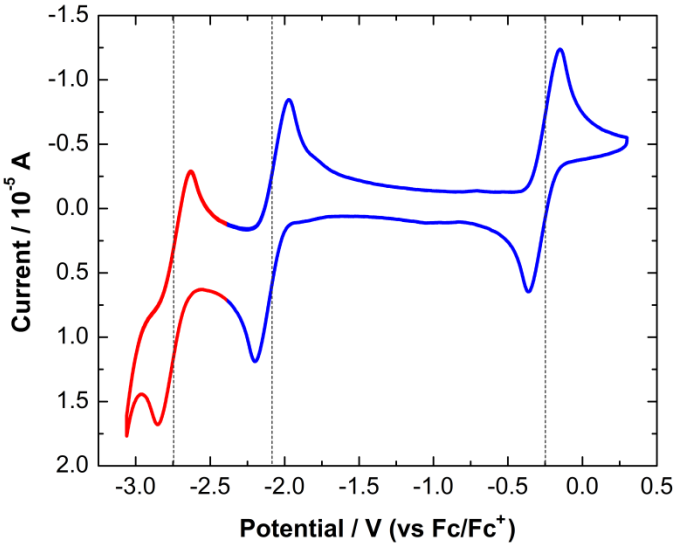

Figure 4. Cyclic voltammogram of **2-COT** in THF (electrolyte = 0.1 M NBu_4PF_6; scan rate = 20 mV s^{-1}). The red and blue regions indicate the reduction and oxidation processes, respectively, from the starting redox state of the neutral complex.

The electronic structures of **1-Bpy** and **1-COT** were also investigated by conducting density functional theory (DFT) calculations on the optimized molecular structure of each complex. For **1-Bpy**, attempts to perform spin stability calculations on the closed shell, non-broken symmetry singlet revealed that this electronic structure did not appear to be the lowest energy state. Further analysis allowed for the identification of a broken symmetry (1,1) minimum that was approximately 20 kJ/mol lower in energy (Figure 5) than the closed shell singlet. We performed

two calculations to assess the relative spin state stability of the **1-COT** complex for the closed-shell singlet and triplet spin states. The singlet was predicted to be the ground state by 51 kJ/mol, with the optimized geometry being a close match to the experimental crystal structure (see Table S5 of the Supporting Information). In the ground state solution, the COT ligand was bound in an η^4-fashion and the unbound planar COT carbon atoms were found to possess alternating bond lengths, as found for the $[COT^{\bullet}]^{-}$ radical anion gas phase geometry.[43] In contrast, the high spin structure was found to possess a planar, η^2-COT ligand with some spin delocalization (~0.3e). Although several calculations were performed with a broken symmetry wavefunction as a starting point with antiferromagnetic spin delocalization onto the COT ligand, the results all returned to the closed shell singlet as the converged solution and therefore offer no support to the experimental spin measurements. A TDDFT calculation[44] was performed to explore any low energy singlet excited states, but the closest state calculated was 2.5 eV higher in energy. A simple Mulliken population analysis revealed a small amount of charge transfer between the Fe and the COT ligand (~0.17e), with the highest occupied molecular orbitals showing considerable overlap between the Fe d-orbitals and an orbital that resembles the HOMO of the $[COT^{\bullet}]^{-}$ radical anion in the gas phase (Figure 6).[43] A calculation of the Mayer bond orders suggests that the unbound COT carbon atoms resemble those of the $[COT^{\bullet}]^{-}$ radical anion; however, the bond order of the central η^4-COT C-C bond was found to be 1.30, supporting the contention of charge transfer into the anti-bonding orbitals of the COT ligands from Fe. The calculated Mössbauer parameters[45] for optimized **1-COT** were found to be δ = 0.09 mm/s and ΔE_Q = 1.33 mm/s and are in fairly good agreement with the measured values. It is possible that our inability to calculate the experimentally observed broken symmetry solution is related to the close proximity of the COT Ψ_3 orbital to the iron center.

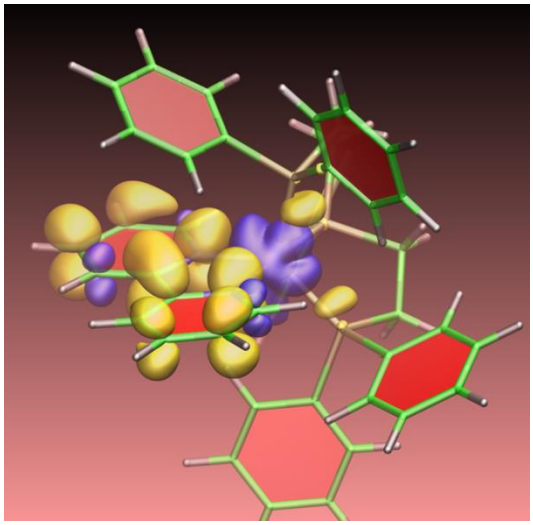

Figure 5. The calculated spin density for the broken symmetry solution found for **1-Bpy**.

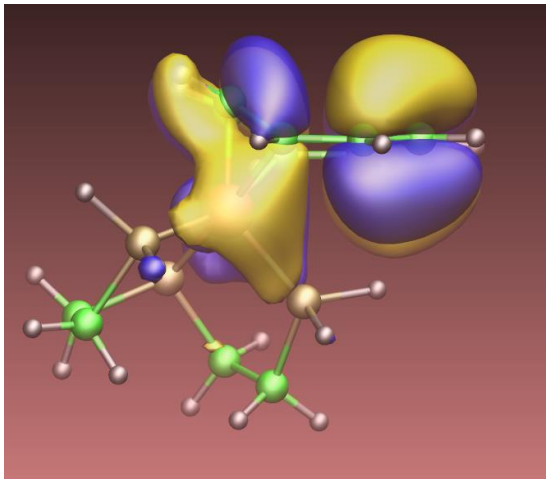

Figure 6. Calculated highest occupied molecular orbital for **1-COT** showing overlap between Fe-d and COT π* orbitals.

Discussion Since Mössbauer and EPR spectroscopic evidence suggests that the electronic structures of **1-COT** and **2-COT** are best described as having low-spin Fe(I) centers that are antiferromagnetically coupled to an η^4-COT radical monoanion, the crystallographically determined C-C and M-C bond distances found for these complexes may be applied as metrics for assessing the degree of η^4-COT ligand reduction present in complexes throughout the d-block. The C(2)-C(3) bond distances determined for **1-COT** and **2-COT** of 1.402(2) and

1.391(4) Å, respectively, are significantly shorter than that of a single C-C bond, and it is believed that a similar bond distance in related complexes could indicate the presence of a COT radical monoanion. In fact, the C(2)-C(3) distances determined for these complexes are even shorter than the range of 1.41-1.43 Å that has recently been described for the central C-C single bond distance associated with bpy radical anion ligands.[11,17] Although less convincing when considered independently, C(1)-C(2) and C(3)-C(4) bond distances of approximately 1.43 Å may also suggest that a given η^4-COT complex features the singly reduced form of this ligand.

Likewise, the M-C bond distances determined for **1-COT** and **2-COT** might indicate the presence of a singly reduced COT ligand in analogous complexes. As shown in Table 5, the M-C(2) and M-C(3) distances found for **1-COT** [2.0302(14) and 2.0330(14) Å, respectively] and **2-COT** [2.047(3) and 2.059(3) Å, respectively] are 0.15-0.20 Å shorter than the distances determined for the neighboring M-C(1) and M-C(4) contacts. With the exception of (η^4-COT)Fe(BAC)$_2$, which features an abnormally long M-C(4) distance, this characteristic is shared with each of the other first row transition metal complexes displayed in Table 5.[36] While it is impractical to reassign the electronic structure of any of these complexes based on crystallographic metrical parameters alone, a particularly interesting comparison can be made between the M-C bond distances determined for **1-COT** or **2-COT** and the homoleptic COT supported Co(I-) complex, [(η^4-COT)$_2$Co][K(2,2,2-crypt)], prepared by Ellis and co-workers.[27] Along with the original publication of this complex, it was proposed that the COT ligands were serving as "superb acceptors" and may be regarded as one-electron oxidizing agents because the complex exhibits an overall square planar coordination geometry.[27] Since the C-C (Table 2) and M-C (Table 5) bond distances determined for [(η^4-COT)$_2$Co][K(2,2,2-crypt)] are very similar to those determined for **1-COT** and **2-COT**,[27] it is believed the electronic structure of [(η^4-COT)$_2$Co][K(2,2,2-crypt)] is likely best described as having a Co(I) center supported by two COT radical anions, as opposed to its formal Co(I-) designation.

Table 5. M-C bond lengths (Å) for complexes featuring η^4-COT coordination.[36]

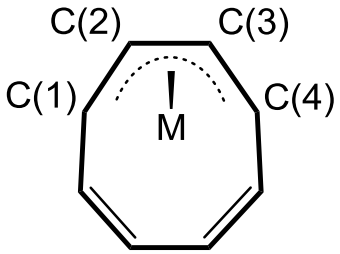

Complex	M-C(1)	M-C(2)	M-C(3)	M-C(4)	Ref.
$[(\eta^4\text{-COT})Cr]_2(\mu\text{-}\eta^5,\eta^5\text{-COT})$	2.369(5)	2.140(4)	2.104(3)	2.279(4)	22
	2.341(3)	2.127(3)	2.112(3)	2.272(3)	
$[(\eta^4\text{-COT})Fe(CO_3)]_2[((\mu\text{-}\eta^1,\eta^1\text{-}(N,N)\text{-2,4-}(CF_3)_2N_2C_3)Ag]_3$	2.190(6)	2.046(5)	2.043(5)	2.187(5)	23
	2.175(5)	2.045(5)	2.059(5)	2.184(6)	
$(\eta^4\text{-COT})Fe(BAC)_2$[a]	2.170(4)	2.066(4)	2.063(4)	2.406(4)	19
$(\eta^4\text{-COT})Fe(\eta^4,\eta^2\text{-cyclooctatriene})_2$[b]	2.1711(11)	2.0295(10)	2.0247(10)	2.2044(11)	19
$(\eta^4\text{-COT})Fe(\mu\text{-}\eta^5,\eta^5\text{-COT})Fe(R)$[c]	2.177(2)	1.985(2)	2.025(3)	2.165(3)	19
(Triphos)Fe(η^4-COT) (**1-COT**)	2.1978(14)	2.0302(14)	2.0330(14)	2.2170(14)	This Work
(Triphos*)Fe(η^4-COT) (**2-COT**)	2.233(3)	2.047(3)	2.059(3)	2.265(3)	This Work
$[(\eta^4\text{-COT})_2Co][K(2,2,2\text{-crypt})]$	2.152(3)	1.991(3)	1.989(3)	2.199(3)	27
$[(\eta^4\text{-COT})Mo]_2(\mu\text{-}\eta^5,\eta^5\text{-COT})$	2.327(5)	2.264(5)	2.271(5)	2.359(6)	31
	2.355(5)	2.241(5)	2.242(6)	2.343(6)	
$[(\eta^5\text{-Cp})Ru(\mu\text{-}\eta^4,\eta^4\text{-COT})(\mu\text{-H})Ru(\eta^5\text{-Cp})][PF_6]$	2.219(2)	2.166(2)	2.166(2)	2.219(2)	33
$[(\eta^5\text{-Cp})Ru]_2(\mu\text{-}\eta^4,\eta^4\text{-COT})$	2.206(3)	2.157(3)	2.163(3)	2.228(3)	33
	2.215(3)	2.164(3)	2.161(3)	2.214(3)	
$[(CO)_2Ru]_2(\mu\text{-}\eta^4,\eta^4\text{-COT})(\mu\text{-}\eta^1,\eta^1\text{-CO})$	2.345(4)	2.240(4)	2.238(4)	2.323(5)	34
$[(\eta^5\text{-Cp})Rh(\mu\text{-}\eta^4,\eta^4\text{-COT})Rh(\eta^2,\eta^2\text{-norbornadiene})][BF_4]$	2.201(4)	2.219(4)	2.219(4)	2.201(4)	35

[a]BAC = *N*,*N*-bis(diisopropyl)aminocyclopropenylidene. [b]The 5- and 8-positions of the cyclooctatriene ring are bridged by a quaternary carbon atom that lies in the 2-position of an *N*-(2,6-diisopropylphenyl)-3,3,5,5-tetramethylpyrrolidine ring. [c]R = 2,4-(*N*,*N*)-bis(2,6-diisopropylphenyl-3,5-diphenylimidazole.

In addition to its potential impact on fundamental electronic structure investigations, the research described herein may also hold implications for the mechanistic study of *N*-heterocyclic carbene promoted COT ligand coupling reactions.[46] In a recent report by Grubbs and co-workers, it was found that the addition of *N*-heterocyclic carbene to two equivalents of $Fe(COT)_2$ allowed

for the isolation of (η^4-COT)Fe(μ-η^5,η^5-COT)Fe(R) [R = 2,4-(*N*,*N*)-bis(2,6-diisopropylphenyl-3,5-diphenylimidazole], which further undergoes radical coupling of two η^4-COT ligands.[19] Although a full electronic structure investigation of this complex with complimentary Mössbauer and EPR spectroscopic data has not been conducted, the solid state structure of (η^4-COT)Fe(μ-η^5,η^5-COT)Fe(R) has been reported to feature C(2)-C(3), Fe-C(2), and Fe-C(3) bond distances of 1.400(3), 1.985(2), and 2.025(3) Å, respectively, along with Fe-C(1) and Fe-C(4) distances of 2.177(2) and 2.165(3) Å, respectively (Table 4).[19] Although the C(1)-C(2) and C(3)-C(4) distances of 1.447(3) and 1.400(4) Å appear to be somewhat unusual, the other COT and Fe-C distances suggest that this complex may feature an η^4-COT radical monoanion, rather than a neutral η^4-COT ligand.[19] While it is impossible to tell which electronic structure assignment is correct without further spectroscopic study, it appears inappropriate to assume that this complex possesses a neutral η^4-COT ligand solely because it exhibits a "localized butadiene" structure within the unbound COT carbon atoms.

In moving beyond the first transition series examples shown in Table 5, it is clear that structurally characterized second row complexes featuring an η^4-COT ligand tend to have M-C(2) and M-C(3) distances that are much closer to their M-C(1) and M-C(4) counterparts. As recently discussed in the investigation of redox non-innocent ligand supported Rh(I)[47] and Mo(0)[48] complexes, it is believed that the second row complexes in Table 5 likely feature electronic structures that are consistent with different degrees of π-backbonding into the η^4-COT ligand rather than having a COT radical anion, since second row metals have d-orbitals that more efficiently overlap with ligand-based π-orbitals than their first row congeners.[49] This characteristic renders it unlikely that population of the COT π^*-orbital[2a] will be achieved, as the resulting π^*-M(4d/5d) antibonding orbital would be highly destabilized relative to the filled orbital associated with π^*-M(4d/5d) bonding.[50]

Concluding Remarks

Two well-characterized organometallic complexes featuring an η^4-COT radical monoanion ligand have been presented. Although DFT calculations were unable to predict a broken symmetry solution for **1-COT**, Mössbauer and EPR spectroscopic investigations, in combination with single crystal X-ray diffraction and cyclic voltammetry studies offered experimental support

for this electronic structure designation. It is believed that the solid state metrical parameters reported herein for both **1-COT** and **2-COT** provide a model for assessing the electronic structure of other first row transition metal complexes that possess an η^4-COT ligand, and perhaps any first row complex that contains an η^4-diene ligand. In turn, revealing the fundamental electronic properties of these complexes may lead researchers to develop an advanced understanding of their reactivity.

Experimental Section

General Considerations: All synthetic reactions were performed in an MBraun or Vacuum Atmospheres glovebox under an atmosphere of purified nitrogen or argon. Aldrich or Acros anhydrous solvents were either sparged with argon or dried using a Pure Process Technology solvent purification system before being stored in the glovebox over activated 4Å molecular sieves (Fischer Scientific) and sodium (Alfa Aesar) before use. Benzene-d_6 and tetrahydrofuran-d_8 were purchased from Cambridge Isotope Laboratories and dried over 4Å molecular sieves prior to use. Bis(cyclooctatetraene) iron(0), bis(2-diphenylphosphinoethyl)phenylphosphine (Triphos), and 1,1,1-Tris(diphenylphosphinomethyl)ethane (Triphos*) were purchased from Strem Chemicals while iron(II) dibromide was purchased from Acros. **1-Br$_2$, 1-κ^2-Triphos**, and **1-Bpy** were prepared according to literature procedure.[17] All of the gases used in this study were obtained from either Airgas or Praxair.

Solution ^{1}H nuclear magnetic resonance (NMR) spectra were recorded at room temperature on either a Bruker AVANCE 400 MHz or Varian MR400 spectrometer. All ^{1}H and ^{13}C NMR chemical shifts are reported relative to $SiMe_4$ using ^{1}H (residual) and ^{13}C chemical shifts of the solvent as secondary standards. ^{31}P NMR data is reported relative to H_3PO_4. Elemental analyses were performed at either Robertson Microlit Laboratories Inc. (Ledgewood, NJ) or on a PerkinElmer 2400 Series elemental analyzer at the Goldwater Environmental Laboratory (Arizona State University). Solid state magnetic susceptibilities were determined at 23 ˚C using a Johnson Matthey magnetic susceptibility balance calibrated with $HgCo(SCN)_4$ and $K_3Fe(CN)_6$.

Single crystals suitable for X-ray diffraction were coated with polyisobutylene oil in a drybox and transferred to a nylon loop which was then mounted on the goniometer head of a Bruker APEX (Arizona State University) or APEX II (Los Alamos National Laboratory) diffractometer

equipped with Mo K_α radiation. A hemisphere routine was used for data collection and determination of the lattice constants. The space group was identified and the data were processed using the Bruker SAINT+ program and corrected for absorption using SADABS. The structures were solved using direct methods (SHELXS), completed by subsequent Fourier synthesis, and refined by full-matrix, least-squares procedures on $|F|^2$ (SHELXL). The crystallographic parameters for **1-COT·C_7H_8** (CCDC–997804), **2-COT** (CCDC–997805), and **1-κ^2-Triphos** (CCDC–997806) are provided in Table S1 of the Supporting Information.

Mössbauer Studies: The presence of Fe in these materials strongly suggests using the Mössbauer Effect (ME) of ^{57}Fe to ascertain detailed properties of the Fe constituents. A ME spectrometer operated in the constant acceleration mode was combined with a liquid helium cryostat, and conventional data analysis programs for ^{57}Fe ME spectra were used. A ^{57}Co in Rh source provided the 14.4 KeV recoil-free ME γ-rays. The samples were contained in an O-ring sealed Lucite holder under an Ar atmosphere. The source and absorber were held at the same temperature for data taken over the range 1.5 to 300 K. Only data and results at 76-77 K are reported here showing one or two Fe sites and their isomer shifts (IS) and quadrupole splittings (ΔE_Q). The IS is related to the electronic state of the Fe, and the ΔE_Q to its ligand environment. Of particular interest in these studies is the magnetic state of the Fe. No spontaneous ordering was observed at any temperature down to 1.5 K. Furthermore, no sample showed any hyperfine relaxation response; the Fe in the reported samples is non-magnetic. The isomer shift data exclude most usual Fe valences and spin values but do not provide an unambiguous assignment of the Fe state from ME data alone.

Electron Paramagnetic Resonance Spectroscopy: *Instrumentation*. Data collection and analysis were performed at the EPR Facility of Arizona State University. Continuous wave EPR spectra were recorded at 70 K using a Bruker ELEXSYS E580 continuous wave X-band spectrometer (Bruker, Silberstreifen, Germany) equipped with an Oxford Model ESR900 liquid helium cryostat (Oxford Instruments, Oxfordshire, UK). The magnetic field modulation frequency was 100 kHz with a field modulation of 0.5 mT peak-to-peak. The microwave power was 4 mW, the microwave frequency was 9.45 GHz and the sweep time was 84 seconds.

Spin Hamiltonian. The EPR spectrum of two $S = 1/2$ spins coupled by isotropic and anisotropic interactions has been extensively discussed. We refer the reader to the main textbooks and reviews for a more comprehensive background.[51-53] The EPR spectrum of **1-COT** was analyzed considering that the molecule contains two $S = 1/2$ spins. One corresponding to the unpaired electron from the low-spin Fe(I) (denoted by $\mathbf{S_A}$) and the other belongs to the unpaired electron at the COT radical (denoted by $\mathbf{S_B}$). They interact with an external magnetic field (Zeeman interaction) and with each other, through exchange and dipole-dipole interactions. The spin Hamiltonian, $\mathcal{H}$, of this system is:

$$\mathcal{H} = \beta_e \mathbf{S_A} \cdot \boldsymbol{g}_\mathbf{A} \cdot \mathbf{B_0} + \beta_e \mathbf{S_B} \cdot \boldsymbol{g}_\mathbf{B} \cdot \mathbf{B_0} + hJ_o \mathbf{S_A} \cdot \mathbf{S_B} + h\mathbf{S_A} \cdot \boldsymbol{J} \cdot \mathbf{S_B} \quad (1)$$

Where $\boldsymbol{g}_\mathbf{A}$ and $\boldsymbol{g}_\mathbf{B}$ are the *g*-tensors of $\mathbf{S_A}$ and $\mathbf{S_B}$, respectively, and β_e is the Bohr magneton. The first two terms are the Zeeman interactions with the applied magnetic field $\mathbf{B_0}$. The third and fourth terms are, respectively, the isotropic (Heisenberg) exchange and the dipole-dipole interactions that couple $\mathbf{S_A}$ with $\mathbf{S_B}$.

Fitting of EPR spectra. To quantitatively compare experimental and simulated spectra, we divided the spectra into N intervals, i.e. we treated the spectrum as an N-dimensional vector **R**. Each component R_j has the amplitude of the EPR signal at a magnetic field B_j, with j varying from 1 to N. The amplitudes of the experimental and simulated spectra were normalized so that the span between the maximum and minimum values of R_j is 1. We compared the calculated amplitudes R_j^{calc} of the signal with the observed values R_j defining a root-mean-square deviation σ by:

$$\sigma(p_1, p_2, \ldots, p_n) = \left[\sum_j \left(R_j^{calc}(p_1, p_2, \ldots, p_n) - R_j^{exp}\right)^2 / N\right]^{1/2} \quad (2)$$

where the sums are over the N values of j, and p's are the fitting parameters that produced the calculated spectrum. For our simulations, N was set equal to 1024.

The EPR spectra were simulated using EasySpin (v 4.5.0), a computational package developed by Stoll and Schweiger[54] and based on Matlab (The MathWorks, Natick, MA, USA). EasySpin

calculates EPR resonance fields using the energies of the states of the spin system obtained by direct diagonalization of the spin Hamiltonian (see Eq. 1). The EPR fitting procedure used a Monte Carlo type iteration to minimize the root-mean-square deviation, σ (see Eq. 2) between measured and simulated spectra. We searched for the optimum values of the following parameters: the principal components of $\boldsymbol{g}_{\mathbf{A}}$ and $\boldsymbol{g}_{\mathbf{B}}$ (i.e. $g_{x\mathrm{A}}$, $g_{y\mathrm{A}}$, $g_{z\mathrm{A}}$ and $g_{x\mathrm{B}}$, $g_{y\mathrm{B}}$, $g_{z\mathrm{B}}$), the isotropic exchange J_{o}, the principal components of the dipole-dipole interaction tensor $\boldsymbol{J}$ (i.e. $J_{x'}$, $J_{y'}$, $J_{z'}$) and the peak-to-peak line-widths (ΔB_x, ΔB_y, and ΔB_z).

Electrochemistry: Electrochemical measurements were run with a BASi Analytical Instruments model EC epsilon potentiostat. A conventional three-electrode setup was used for both cyclic voltammetry and differential pulse voltammetry, with a glassy carbon working electrode, a Pt-wire auxiliary electrode, and a Ag-wire as pseudo-reference electrode. Ferrocene was used as an internal reference and all potentials herein are reported vs Fc/Fc^{+}. Extra dry, deoxygenated THF was used as solvent to prepare sample solutions. All measurements were made in a glovebox under inert atmosphere (Ar) at room temperature.

Electronic Structure Calculations: Density functional theory (DFT) calculations were carried out with the Gaussian 09 software (revision B.01)[55] and the ORCA software.[56] Geometry optimization calculations were carried out for the complexes using the crystal structures as starting points with the phenyl groups replaced by hydrogens to reduce the computational expense. The PBE exchange correlation functional (PBE exchange and PBE correlation)[57] was used for all calculations using a LANL2DZ basis set (5s5p3d+f) for Fe[58] with a 6-31G* basis set for all other elements using the spin-unrestricted molecular orbital approach. The LANL2DZ effective core potential was used for Fe. Wavefunction stability tests were employed to ensure that the calculated wavefunction corresponds to the true electronic ground state. Time-dependent density functional theory calculations were also calculated with the Gaussian 09 software to search for low energy singlet excited states. Atomic spin densities and charges were evaluated using a Mulliken population analysis. Several calculations were repeated using the B3LYP functional[59] to ensure that the same general trends in the results were not dependent on the

functional used. The ORCA software[56] was used to determine Mayer bond orders and to calculate the Mössbauer parameters for the complexes.[45]

Preparation of [κ^3-PhP($CH_2CH_2PPh_2$)$_2$]Fe(η^4-C_8H_8) (1-COT). Method A: In the glovebox, a 20 mL scintillation vial was charged with 0.020 g (0.076 mmol) of Fe(COT)$_2$ and approximately 1 mL of benzene-d_6. While stirring, a solution of 0.040 g (0.075 mmol) Triphos in approximately 1 mL of benzene-d_6 was added dropwise. After approximately 1 min, an aliquot of the solution was taken and filtered through Celite into a J. Young tube. After 10 min, analysis of this aliquot by ^{1}H and ^{31}P NMR spectroscopy revealed that the reaction was near completion. Upon confirming spectroscopically that the reaction was complete after 1 hour, the fractions were recombined, filtered through Celite, and the solvent was evacuated to yield a red solid. After washing with 1 mL of pentane and 1 mL of Et_2O to remove a small amount of residual Triphos, 0.021 g (0.030 mmol, 40% yield) of **1-COT** was collected. **Method B:** A 100 mL round-bottomed flask was charged with 0.213 g of **1-Br$_2$** (0.284 mmol), 0.592 g (5.690 mmol) of 1,3,5,7-cyclooctatetraene (COT), and approximately 80 mL of diethyl ether. This slurry was placed in a -35 °C freezer for 20 minutes. After this time, freshly cut sodium metal (0.033 g, 1.422 mmol) was added to the slurry while cold. The reaction was set to stir while warming to room temperature. After 15 h, the resulting deep red solution was filtered through Celite and the Celite pad was washed with 15 mL of toluene to fully wash down the product. The solvent was evacuated to yield a red solid. This material was washed 5 times with pentane (5 x 10 mL) to get rid of excess COT. Then it was washed five times with diethyl ether (5 x 5 mL) to remove any remaining free ligand. Recrystallization from a diethyl ether-layered toluene solution yielded 0.098 g (0.141 mmol, 49%) of a red solid identified as **1-COT**. Conducting this reaction with 10 eq. rather than 20 eq. of 1,3,5,7-cyclooctatetraene in tetrahydrofuran afforded a 1:1 ratio of **1-COT** to **1-κ^2-Triphos**. Analysis for $C_{42}H_{41}FeP_3$: Calcd. C, 72.63%; H, 5.95%; Found: C, 72.31% H, 5.66%. Magnetic Susceptibility: μ_{eff} = 0.8 μ_B (Evan's Method, 25 ^{o}C, toluene-d_8), μ_{eff} = 0.0 μ_B (Evan's Method, -60 ^{o}C, toluene-d_8). ^{1}H{^{31}P} NMR (benzene-d_6): δ (ppm) = 7.79 (t, J = 7.6 Hz, 2H, *phenyl*), 7.31 (t, J = 7.4 Hz, 2H, *phenyl*), 7.23 (t, J = 7.4 Hz, 1H, *phenyl*), 7.09 (t, J = 7.4 Hz, 4H, *phenyl*), 7.03 (m, 6H, *phenyl*), 6.88 (d, J = 7.0 Hz, 10H, *phenyl*), 4.93 (s, 8H, *COT*), 2.16 (m, 2H, -CH_2), 1.91 (m, 4H, -CH_2), 1.01 (m, 2H, -CH_2). ^{13}C NMR (benzene-d_6): δ (ppm) = 132.9 (m,

phenyl), 132.5 (m, *phenyl*), 131.4 (m, *phenyl*), 129.7 (s, *phenyl*), 129.4 (s, *phenyl*), 129.1 (s, *phenyl*), 129.0 (s, *phenyl*), 128.9 (s, *phenyl*), 128.7 (s, *phenyl*), 128.4 (m, *phenyl*), 128.2 (m, *phenyl*), 127.2 (m, *phenyl*), 95.8 (s, *COT*), 32.22 (m, P*C*H_2*C*H_2P). $^{31}P\{^1H\}$ NMR (benzene-d_6): δ (ppm) = 116.33 (t, J = 7.8 Hz, Fe-*P*Ph), 95.71 (d, J = 7.8 Hz, Fe-*P*Ph_2).

Preparation of [$H_3CC(CH_2PPh_2)_3$]$FeBr_2$ (2-Br_2): In the glove box a 20 mL scintillation vial was charged with $FeBr_2$ (0.094 g, 0.435 mmol), Triphos* (0.271 g, 0.435 mmol) and approximately 15 mL of tetrahydrofuran. The resulting solution was set to stir at room temperature for six hours while it turned faint yellow in color. It was filtered through Celite and the solvent was evacuated to obtain a glassy film at the bottom of the filter flask, which was scraped with pentane, which was then decanted, twice (2 x 5 mL). Drying *in vacuo* yielded 0.310 g of a glassy solid (85%), identified as **2-Br_2**. Analysis for $C_{41}H_{39}FeBr_2P_3$: Calcd. C, 58.60%; H, 4.68%; Found: C, 58.57% H, 4.64%. Magnetic Susceptibility (Gouy Balance, 26 ^oC): μ_{eff} = 4.4 μ_B. ^1H NMR (tetrahydrofuran-d_8): δ (ppm) = 139.89 (peak width at ½ height = 5660 Hz), 57.61 (4590 Hz), 13.02 (735 Hz), 5.63 (321 Hz). ^{31}P NMR (tetrahydrofuran-d_8): δ (ppm) = 21.91 (2651 Hz).

Preparation of [κ^3-$(Ph_2PCH_2)_3C(CH_3)$]Fe[COT] (2-COT): A 100 mL round-bottomed flask was charged with 0.198 g of **2-Br_2** (0.236 mmol), 0.086 g (0.828 mmol) of 1,3,5,7-cyclooctatetraene (COT), and approximately 50 mL of diethyl ether. This slurry was placed in a -35 °C freezer for 25 minutes. After this time, freshly cut sodium metal (0.027 g, 1.182 mmol) was added to the slurry while cold. The reaction was set to stir while warming to room temperature. After 15 h, the resulting deep reddish-brown solution was filtered through Celite and the Celite pad was washed with 15 mL of toluene. The solvent was evacuated to yield a reddish-brown solid. This material was washed 5 times with pentane (5 x 10 mL) to get rid of excess COT and dried under vacuum. The red solid was then dissolved in approximately 15 mL toluene and filtered through a Celite column. After evaporating the toluene, the red solid was washed five times with diethyl ether (5 x 4 mL) and it was dried under vacuum to obtain 0.080 g (0.102 mmol, 43%) of red crystals identified as **2-COT**. This complex was also prepared following the straightforward addition of Triphos* to $Fe(COT)_2$. Analysis for $C_{49}H_{47}FeP_3$: Calcd.

C, 75.00%; H, 6.04%. Found: C, 74.64%; H, 6.28%. Magnetic Susceptibility: μ_{eff} = 0.9 μ_B (Evan's Method, 25 ^oC, toluene-d_8), μ_{eff} = 0.0 μ_B (Evan's Method, -60 ^oC, toluene-d_8). ^1H NMR (benzene-d_6): δ (ppm) = 6.93 (m, 18 H, *phenyl*), 6.82 (m, 12H, *phenyl*), 5.53 (s, 8H, *COT*), 2.00 (broad m, 6H, -CH_2), 0.993 (broad s, 3H, -CH_3). ^{13}C NMR (benzene-d_6): δ (ppm) = 143.5 (m, *phenyl*), 133.1 (m, *phenyl*), 128.0 (m, *phenyl*), 128.3 (m, *phenyl*), 95.7 (s, COT), 39.9 (m, CH_2P), 37.9 (m, CCH_3), 35.9 (m, CH_3). $^{31}P\{^1H\}$ NMR (benzene-d_6): δ (ppm) = 53.35 (s, *Fe-P*Ph_2).

Supporting Information.

Crystallographic parameters, Mössbauer and multinuclear NMR spectra. This material is available free of charge via the Internet at http://pubs.acs.org.

Acknowledgement:

We would like to thank the LANL Laboratory Directed Research and Development Program for financial support. Additionally, we would like to acknowledge Dr. Thomas L. Groy (ASU) for his assistance with X-ray crystallography and Dr. Owen Summerscales (LANL) for helpful discussions regarding COT coordination chemistry. This research used resources provided by the Los Alamos National Laboratory Institutional Computing Program, which is supported by the U.S. Department of Energy National Nuclear Security Administration under Contract No. DE-AC52-06NA25396.

References

[1] (a) Cotton, F. A. *Chem*. *Rev*. **1955**, *55*, 551-594, and references therein. (b) Cotton, F. A. *Inorg*. *Chem*. **2002**, *41*, 643-658.

[2] (a) Crabtree, R. H. *The Organometallic Chemistry of the Transition Metals*; John Wiley & Sons: Hoboken, NJ, 2009. (b) Collman, J. P.; Hegedus, L. S.; Norton, J. R.; Finke, R. G. *Principals and Applications of Organotransition Metal Chemistry*; University Science Books: Sausalito, CA, 1987. (c) Pettit, R.; Emerson, G. F. *Adv*. *Organomet*. *Chem*. **1964**, *1*, 1-46. (d) Summerscales, O. T.; Cloke, F. G. N. *Coord*. *Chem*. *Rev*. **2006**, *250*, 1122-1140.

[3] (a) Yasuda, H.; Nakamura, A. *Angew*.*Chem*. *Int*. *Ed*. *Engl*. **1987**, *26*, 723-742. (b) Yasuda, H.; Tatsumi, K.; Nakamura, A. *Acc*. *Chem*. *Res*. **1985**, *18*, 120-126.

[4] (a) For extended Hückel calculations on (η^4-2,3-dimethyl-1,3-butadiene)$_3$Mo see: Yun, S. S.; Kang, S. K.; Suh, I-H.; Choi, Y. D.; Chang, I. S. *Organometallics* **1991**, *10*, 2509-2512. (b) For a DFT study on (η^4-1,3-butadiene)Fe(CO)$_2$(L) (L = CO, PH_3, PMe_3) see González-Blanco, Ò.; Branchadell, V. *Organometallics* **1997**, *16*, 475-481.

[5] Bosch, M.; Laubender, M.; Weberndörfer, B.; Werner, H. *Chem. Eur. J.* **1999**, *5*, 2203-2211.

[6] (a) Khan, M. A.; Mahon, M. F.; Stewart, A. J. W.; Lewis, S. E. *Organometallics* **2010**, *29*, 199-204. (b) Knölker, H.-J. *Chem. Rev.* **2000**, *100*, 2941-2961, and references therein.

[7] (a) Schnöckelborg, E-M.; Khusniyarov, M. M.; de Bruin, B.; Hartl, F.; Langer, T.; Eul, M.; Schultz, S.; Pöttgen, R.; Wolf, R. *Inorg. Chem.* **2012**, *51*, 6719-6730. (b) Brodt, C.; Niu, S.; Pritkow, H.; Stephan, M.; Zenneck, U. *J. Organomet. Chem.* **1993**, *459*, 283-291. (c) Thompson, R. L.; Lee, S.; Rheingold, A. L.; Cooper, N. J. *Organometallics* **1991**, *10*, 1657-1659.

[8] Bennett, M. A. *Adv. Organomet. Chem.* **1966**, *4*, 353-387.

[9] For an example of η^2- and η^3-COT coordination to Sn see: Summerscales, O. T.; Wang, X.; Power, P. P. *Angew. Chem. Int. Ed.* **2010**, *49*, 4788-4790.

[10] (a) Evans, W. J.; Champagne, T. M.; Davis, B. L.; Allen, N. T.; Nyce, G. W.; Johnston, M. A.; Lin, Y.-C.; Khvostov, A.; Ziller, J. W. *J. Coord. Chem.* **2006**, *59*, 1069-1087. (b) Panda, T. K.; Gamer, M. T.; Roesky, P. W. *Inorg. Chem.* **2006**, *45*, 910-916. (c) Roesky, P. W.; Gamer, M. T.; Marinos, N. *Chem. -Eur. J.* **2004**, *10*, 3537-3542. (d) Cendrowski-Guillaume, S. M.; Nierlich, M.; Ephritikhine, M. *J. Organomet. Chem.* **2002**, *643-644*, 209-213. (e) Berthet, J. C.; Nierlich, M.; Ephritikhine, M. *Eur. J. Inorg. Chem.* **2002**, 850. (f) Wetzel, T. G.; Dehnen, S.; Roesky, P. W. *Organometallics* **1999**, *18*, 3835-3842. (g) Schumann, H.; Winterfield, J.; Gorlitz, F. H.; Pickardt, J. *J. Chem. Soc., Chem. Commun.* **1993**, 623-625. (h) Arliguie, T.; Baudry, D.; Ephritikhine, M.; Nierlich, M.; Lance, M.; Vigner, J. *J. Chem. Soc., Dalton Trans.* **1992**, 1019-1024.

[11] Scarborough, C. C.; Wieghardt, K. *Inorg. Chem.* **2011**, *50*, 9773-9793.

[12] Lu, C. C.; Weyhermüller, T.; Bill, E.; Wieghardt, K. *Inorg. Chem.* **2009**, *48*, 6055-6064.

[13] Knijnenburg, Q.; Gambarotta, S.; Budzelaar, P. H. M. *Dalton Trans.* **2011**, *50*, 9879-9887.

[14] (a) Poremba, P.; Schmidt, H-G.; Noltemeyer, M.; Edelmann, F. T. *Organometallics* **1998**, *17*, 986-988. (b) Sygula, A.; Fronczek, F. R.; Rabideau, P. W. *J. Organomet. Chem.* **1996**, *526*, 389-391. (c) Hu, N.; Gong, L.; Jin, Z.; Chen, W. *J. Organomet. Chem.* **1988**, *352*, 61-66. (d) Jones,

M. T.; de Boer, E. *Mol*. *Phys*. **1982**, *47*, 487-499. (e) Noordik, J. H.; van den Hark, T. E. M.; Mooij, J. J.; Klassen, A. A. K. *Acta Cryst*. **1974**, *B30*, 833-835.

[15] Dickens, B.; Lipscomb, W. N. *J. Chem*. *Phys*. **1962**, *37*, 2084-2093.

[16] For a discussion on the electrochemical reduction of COT and COT-coordinated complexes see: (a) Moraczewski, J.; Geiger, Jr.; W. E. *J. Am*. *Chem*. *Soc*. **1981**, *103*, 4779-4787. (b) Baik, M.-H.; Schauer, C. K.; Ziegler, T. *J. Am. Chem. Soc.* **2002**, *124*, 11167-11181, and references therein.

[17] Mukhopadhyay, T. K.; Feller, R. K.; Rein, F. N.; Henson, N. J.; Smythe, N. C.; Trovitch, R. J.; Gordon, J. C. *Chem*. *Commun*. **2012**, *48*, 8670-8672.

[18] Felkin, H.; Lednor, P. W.; Normant, J.-M.; Smith, R. A. J. *J. Organomet*. *Chem*. **1978**, *157*, C64-C66.

[19] Lavallo, V.; El-Batta, A.; Bertrand, G.; Grubbs, R. H. *Angew*. *Chem*. *Int*. *Ed*. **2011**, *50*, 268-271.

[20] O'Connor, J. M.; Hiibner, K.; Closson, A. Gantzel, P. *Organometallics* **2001**, *20*, 1482-1485.

[21] (a) Dimmer, J.-A.; Wesemann, L. *Eur*. *J*. *Inorg*. *Chem*. **2011**, 235-240. (b) Guilera, G.; McGrady, G. S.; Steed, J. W.; Burchell, R. P. L.; Sirch, P.; Deeming, A. J. *New J. Chem*. **2008**, *32*, 1573-1581. (c) Gädt, T.; Schappacher, F. M.; Pöttgen, R.; Wesemann, L. *Inorg*. *Chem*. **2007**, *46*, 2864-2869. (d) Gädt, T.; Eichele, K.; Weremann, L. *Organometallics* **2006**, *25*, 3904-3911. (e) Guilera, G.; McGrady, G. S.; Steed, J. W.; Kaltsoyannis, N. *New J. Chem*. **2004**, *28*, 444-446. (f) Jacob, V.; Huttner, G.; Kaifer, E.; Kircher, P.; Rutsch, P. *Eur*. *J*. *Inorg*. *Chem*. **2001**, 2783-2795. (g) Jacob, V.; Mann, S.; Huttner, G.; Walter, O.; Zsolnai, L.; Kaifer, E.; Rutsch, P.; Kircher, P.; Bill, E. *Eur*. *J*. *Inorg*. *Chem*. **2001**, 2625-2640.

[22] Brauer, D. J.; Krüger, C. *Inorg*. *Chem*. **1976**, *15*, 2511-2514.

[23] Tsupreva, V. N.; Titov, A. A.; Filippov, O. A.; Bilyachenko, A. N.; Smol'yakov, A. F.; Dolgushin, F. M.; Agapkin, D. V.; Godovikov, I. A.; Epstein, L. M.; Shubina, E. S. *Inorg*. *Chem*. **2011**, *50*, 3325-3331.

[24] Karlin, K. D.; Moisan, M. P.; Kustyn, M.; Dahlstrom, P. L.; Zubieta, J.; Raithby, P. R. *Cryst*. *Struct*. *Commun*. **1982**, *11*, 1945-1949.

[25] Bassi, I. W.; Scordamaglia, R. *J. Organomet*. *Chem*. **1972**, *37*, 353-359.

[26] Yu, Y.; Sun, J.; Chen, J. *J. Organomet. Chem*. **1997**, *533*, 13-23.

[27] Brennessel, W. W.; Young, Jr.; V. G.; Ellis, J. E. *Angew. Chem. Int. Ed.* **2002**, *41*, 1211-1215.

[28] Rogers, D. M.; Wilson, S. R.; Girolami, G. S. *Organometallics* **1991**, *10*, 2419-2424.

[29] Brauer, D. J.; Krüger, C. *J. Organomet. Chem.* **1972**, *42*, 129-137.

[30] Sinnema, P. J.; Meetsma, A.; Teuben, J. H. *Organometallics* **1993**, *12*, 184-189.

[31] Cotton, F. A.; Koch, S. A.; Schultz, A. J.; Williams, J. M. *Inorg. Chem.* **1978**, *17*, 2093-2098.

[32] Cotton, F. A.; Eiss, R. *J. Am. Chem. Soc.* **1969**, *91*, 6593-6597.

[33] Heck, J.; Lange, G.; Malessa, M.; Boese, R.; Bläser, D. *Chem. –Eur. J.* **1999**, *5*, 659-668.

[34] Brown, D. B.; Johnson, B. F. G.; Martin, C. M.; Parsons, S. *J. Organomet. Chem.* **1997**, *536-537*, 285-291.

[35] Bieri, J. H.; Egolf, T.; van Philipsborn, W.; Piantini, U.; Prewo, R.; Ruppli, U.; Salzer, A. *Organometallics* **1986**, *5*, 2413-2425.

[36] For the purposes of this contribution, a C-C bond metrical parameter error limit of ±0.01 Å has been set for inclusion of a data set in electronic structure discussion.

[37] (a) Dierks, V. H.; Dietrich, H. *Acta Cryst., Sect. B.* **1968**, *24*, 58-62. (b) Dietrich, H.; Dierks, H. *Angew. Chem. Int. Ed.* **1966**, *5*, 899.

[38] Boynton, J. N.; Summerscales, O. T.; Grandjean, F.; Long, G. J.; Fettinger, J. C.; Power, P. P. *Organometallics* **2012**, *31*, 8559-8560.

[39] Farmery, K.; Kilner, M.; Greatrex, R.; Greenwood, N. N. *J. Chem. Soc. A* **1969**, 2339-2345.

[40] Dickson, D. P. E.; Berry, F. J. *Mössbauer Spectroscopy*, Cambridge University Press: Trowbridge, Great Britain, 1986.

[41] Hanson, A. W. *Acta Cryst.* **1962**, *15*, 930-933.

[42] Calvo, R.; Isaacson, R. A.; Paddock, M. L.; Abresch,E. C.; Okamura,M. Y.; Maniero, A. L.; Brunel, L. C.; Feher G. *J. Phys. Chem. B.* **2001**, *105*, 4053-4057.

[43] Klärner, F.-G. *Angew. Chem. Int. Ed.* **2001**, *40*, 3977-3981, and references therein.

[44] Stratman, R. E.; Scuseria, G. E.; Frisch, M. J. *J. Chem. Phys.* **1998**, *109*, 8218-8224.

[45] Römelt, M.; Ye, S.; Neese, F. *Inorg. Chem.* **2009**, *48*, 784-785.

[46] Lavallo, V.; Grubbs, R. H. *Science* **2009**, *326*, 559-562.

[47] Ben-Daat, H.; Hall, G. B.; Groy, T. L.; Trovitch, R. J. *Eur. J. Inorg. Chem.* **2013**, 4430-4442.

[48] Pal, R.; Groy, T. L.; Bowman, A. C.; Trovitch, R. J. *Inorg. Chem.* **2014**, *53*, 9357-9365.

[49] (a) Huheey, J. E. *Inorganic Chemistry: Principles of Structure and Reactivity*; 3rd ed., Harper & Row, New York, **1983**, pp. 368-458. (b) Burdett, J. K. *Chemical Bonds: A Dialog*; John Wiley & Sons: Chichester, England, **1997**, pp. 33-39 and pp. 54-66.

[50] (a) Albright, T. A.; Burdett, J. K.; Whangbo, M.-H. *Orbital Interaction in Chemistry*; John Wiley & Sons: New York, **1985**, pp. 343-347. (b) Albright, T. A.; Burdett, J. K. *Problems in Molecular Orbital Theory*; Oxford University Press, New York, **1992**, pp. 205-206.

[51] Abragam, A.; Bleaney, B. *Electron Paramagnetic Resonance of Transition Ions*; Clarendon Press: Oxford, **1970**, Chapter 9.

[52] Bencini, A.; Gatteschi, D. *Electron Paramagnetic Resonance of Exchange Coupled Systems*; Springer: Berlin, **1990**, Chapter 3.

[53] Eaton, G. R.; Eaton, S. S. In *Biological Magnetic Resonance*; Berliner, L. J., Reuben, J., Eds.; Plenum: New York, **1989**, Vol. 8, pp 339-396.

[54] Stoll, S.; Schweiger A. *J. Magn. Reson*. **2006**, 178, 42-55.

[55] Frisch, M. J.; Trucks, G. W.; Schlegel, H. B.; Scuseria, G. E.; Robb, M. A.; Cheeseman, J. R.; Scalmani, G.; Barone, V.; Mennucci, B.; Petersson, G. A.; Nakatsuji, H.; Caricato, M.; Li, X.; Hratchian, H. P.; Izmaylov, A. F.; Bloino, J.; Zheng, G.; Sonnenberg, J. L.; Hada, M.; Ehara, M.; Toyota, K.; Fukuda, R.; Hasegawa, J.; Ishida, M.; Nakajima, T.; Honda, Y.; Kitao, O.; Nakai, H.; Vreven, T.; Montgomery, Jr., J. A.; Peralta, J. E.; Ogliaro, F.; Bearpark, M.; Heyd, J. J.; Brothers, E.; Kudin, K. N.; Staroverov, V. N.; Kobayashi, R.; Normand, J.; Raghavachari, K.; Rendell, A.; Burant, J. C.; Iyengar, S. S.; Tomasi, J.; Cossi, M.; Rega, N.; Millam, J. M.; Klene, M.; Knox, J. E.; Cross, J. B.; Bakken, V.; Adamo, C.; Jaramillo, J.; Gomperts, R.; Stratmann, R. E.; Yazyev, O.; Austin, A. J.; Cammi, R., Pomelli, C.; Ochterski; J. W.; Martin, R. L.; Morokuma, K.; Zakrzewski, V. G.; Voth, G. A.; Salvador, P.; Dannenberg, J. J.; Dapprich, S.; Daniels, A. D.; Farkas, O.; Foresman, J. B., Ortiz, J. V.; Cioslowski, J.; Fox, D. J. Gas *Gaussian 09 Revision B.01*, Wallingford, CT, Gaussian Inc., 2009.

[56] Neese, F. *WIREs Comput. Mol. Sci.* **2012**, *2*, 73-78.

[57] Perdew, J. P.; Burke, K.; Ernzerhof, M. *Phys. Rev. Lett.* **1996**, *77*, 3865-3868.

[58] Roy, L. E.; Hay, J.; Martin, R. L. *J. Chem. Theory Comput.* **2008**, *4*, 1029-1031.

[59] Becke, A. D. *J. Chem. Phys.* **1993**, *98*, 5648-5652.

Table of Contents Graphic: